Composite Structures 92 (2010) 964–972

Contents lists available at ScienceDirect

Composite Structures

journal homepage: www.elsevier.com/locate/compstruct

Multi-coating inhomogeneities approach for the effective thermo-electro-elastic properties of piezoelectric composite materials

Yao Koutsawa [a], Fabio Biscani [a,b], Salim Belouettar [a,*], Houssein Nasser [a], Erasmo Carrera [b]

[a] Centre de Recherche Public Henri Tudor, 29, Avenue John F. Kennedy, L-1855 Luxembourg, Luxembourg
[b] Department of Aerospace Engineering, Politecnico di Torino, Torino, Italy

ARTICLE INFO

Article history:
Available online 29 September 2009

Keywords:
Micro-mechanics
Thermo-electro-elastic properties
Multi-coated inhomogeneities
Composites

ABSTRACT

This work presents a micromechanics-based model to predict the effective thermo-electro-elastic properties of a piezoelectric composite materials containing ellipsoidal multi-coated inhomogeneities. A finite element analysis is also performed for two-phase piezoelectric composite materials using ABAQUS finite element software. The results obtained from the multi-coating homogenization method show good agreement with the existing experimental results and the finite element results. The inhomogeneities's shape effect as well as the poling direction and the coating effects are investigated. The results show that a proper choice of materials and inhomogeneities's geometry can lead to the desired thermo-electro-elastic properties.

1. Introduction

Functional piezoelectric composite materials have been rapidly developing with increasing applications in ultrasonic imaging devices, sensors, actuators and transducers etc. Such composites inherit the characteristics of functional materials, such as the piezoelectric and piezomagnetic properties which can be tailored to meet specific applications.

Historically, improvements in piezoelectric materials have been focused on the development of single phase materials. Typical examples include piezoelectric ceramics such as lead zirconate-titanate (PZT), and piezoelectric polymers such as polyvinylidene difluoride (PVDF). However, it is now clear that single phase piezoelectric materials can only partially meet the desired requirements such as high strength, low thermal expansion coefficients, high thermal conductivities, and low dielectric constants for many new transducers and sensors. It has been shown that some composite materials can provide superior properties compared to their mother monolithic constituent materials. It has been proved in [1,2] that the piezo-composites can provide a higher piezoelectric strain modulus d_{31} than the constituents. Also, numerical results in [3] showed that the effective thermal expansion coefficients of composites could significantly exceed those of the matrix and the fiber phases.

In an effort to obtain piezoelectric materials with the competing properties, many conventional piezoelectric materials are engineered to incorporate inclusions, and in some cases even voids, to achieve the desired thermo-electro-elastic properties. Combining two or more distinct constituents, piezoelectric composite materials can take the advantages of each constituent since an important application of composite structures is the use of the product property, which is found in the composite structures but is absent in the individual phases [4]. However, the introduction of inclusions or voids into base media will generally lead to the material being anisotropic, complicated and, in some situations, even detrimental to the performance of the composite. Therefore, in order for the composite to offer a favorable behavior, it is necessary to clearly examine the thermo-electro-elastic responses from a micromechanics point of view so that the influence of each material parameter can be understood thoroughly [5]. Different techniques have been adopted in the literature for estimating of the effective properties of piezoelectric composites. The most significant works in this area are those in Refs. [6–8,3,9], among others.

Most of the time these techniques are obtained as extension of the ones developed for pure elastic materials. In the framework of the uniform field methods, Tan and Tong [10] derived closed-form formulas for the effective properties using the iso-field assumptions and multiple loading condition. Aboudi extended the generalized method of cells to piezoelectric materials in [11] by imposing mechanical equilibrium and Maxwell's charge equation in the constituent regions in conjunction with the continuity of mechanical displacements, tensions, electric potential and electric displacements. Bravo-Castillero et al. [12] extended the asymptotic homogenization method to piezoelectric materials. Tang and Yu [13], starting from the total electric enthalpy of the heterogeneous continuum, formulate a micromechanics model as a constrained minimization problem using the variational asymptotic method and

* Corresponding author. Tel.: +352 54 55 80 530; fax: +352 42 59 91 333 (S. Belouettar).
E-mail address: salim.belouettar@tudor.lu (S. Belouettar).

0263-8223/$ - see front matter © 2009 Elsevier Ltd. All rights reserved.
doi:10.1016/j.compstruct.2009.09.041

implement it using the finite element method. Two different models that belong to the same family of the model presented in this paper can be found in [14,15]. Both are based on the self-consistent model: Tong et al. [14] consider a three-phase cylindrical model for analyzing fiber composite, whereas Levin et al. [15] are concerned with composite materials that consist of a homogeneous matrix phase with a set of inclusions uniformly distributed in the matrix.

Inspired by the above interesting and exciting modeling tools as well as by the excellent designability of composites including piezoelectric composites, scientists and engineers begin to pursue the optimal design for the desired applications. With the rapid advancement in technological research, it is expected that composites and completely novel materials could be conveniently designed and manufactured by direct engineering of their constituents [16,14]. In this work, the multi-coating micromechanical model introduced in [17,18] for elastic and viscoelastic composite materials is extended to the effective thermo-electro-elastic properties of piezoelectric composite materials containing multi-coated inhomogeneities. This paper is organized as follows. Section 2 presents the micromechanical model. Firstly the constitutive equations, the notations adopted and the topology of the problem are introduced. Then the integral equations and the localization pseudo-tensors are derived. Finally two homogenization schemes to compute the effective properties are shown. In Section 3, following the works in [19,20], a finite element homogenization method is presented for the effective thermo-electro-elastic properties of two-phase piezo-composites with ellipsoidal inhomogeneities. Section 4 shows results obtained with the proposed model in comparison with results from the finite element homogenization and with experimental data found in the literature [21,22]. The effects of the inhomogeneities shape, the poling direction and the coating are also investigated.

2. Micromechanical model

2.1. Constitutive equations, notations and topology

The constitutive equations for the stationary linear response of a thermo-electro-elastic material can be expressed as:

$$\begin{cases} \sigma_{ij} = C^E_{ijkl}\varepsilon_{kl} - e_{kij}E_k - \beta_{ij}\Delta T, \\ D_i = e_{ikl}\varepsilon_{kl} + \kappa^{\varepsilon}_{ik}E_k - \pi_i\Delta T, \\ h_i = k_{ij}e_j. \end{cases} \tag{1}$$

Here σ_{ij} and ε_{kl} are the components of the stress and the strain tensors, E_i and D_i are the components of the electric field and the electric displacement vectors, h_i and e_j are the components of the thermal flux and of the heat strain vectors, C^E_{ijmn} are the components of the elastic modulus tensor measured at a constant electric field and temperature, $\kappa^{\varepsilon}_{ik}$ are the components of the dielectric tensor at fixed strain and temperature, e_{kmn} are the components of the piezoelectric constants tensor measured at fixed temperature and strain or electric field, k_{ij} are the components of the thermal conductivity tensor, β_{ij} and π_i represent the components of the temperature stress coefficients tensor and the components of the pyroelectric constants vector measured at fixed strain and electric field and finally ΔT denotes the temperature change from a reference temperature. In the calculation of the effective temperature stress coefficients and the pyroelectric constants we assume that the temperature field, obtained by solving an uncoupled problem of heat-conduction, is not affected by mechanical and electrical fields. Moreover the calculation of the thermal conductivity tensor is decoupled from the electro-mechanical problem.

Extending the shorthand notation introduced in many works such as [23,9], the thermo-electro-elastic constants can be expressed on equal footing in the following as

$$L_{iJMn} = \begin{cases} C^E_{ijmn}, & J,M = 1,2,3, \\ e_{nij}, & J = 1,2,3; M = 4, \\ e_{imn}, & M = 1,2,3; J = 4, \\ -\kappa^{\varepsilon}_{in}, & J = M = 4, \\ k_{in}, & J = M = 5, \\ 0, & \text{elsewhere}, \end{cases} \quad \text{and} \quad \beta_{mN} = \begin{cases} \beta_{mn}, & N = 1,2,3, \\ \pi_m, & N = 4, \\ 0, & N = 5. \end{cases} \tag{2}$$

With this shorthand notation, the linear constitutive Eqs. (1) can be unified into the single equation as

$$\Sigma_{iJ} = L_{iJKl}Z_{Kl} - \beta_{ij}\Delta T, \tag{3}$$

where

$$\Sigma_{iJ} = \begin{cases} \sigma_{ij}, & J = 1,2,3, \\ D_i, & J = 4, \\ h_i, & J = 5, \end{cases} \quad \text{and} \quad Z_{Kl} = \begin{cases} \varepsilon_{kl}, & K = 1,2,3, \\ -E_l, & K = 4, \\ e_l, & K = 5. \end{cases} \tag{4}$$

In the preceding equations and in what follows the summation convention applies to repeated Latin subscripts and the comma denotes partial differentiation. The lowercase Latin subscripts range from 1 to 3 while the uppercase subscripts range from 1 to 5. Vectors or tensors hereafter are shown in bold face. In Eq. (4) the elastic strain, the electric field and the thermal strain are derivable from

$$U_M = \begin{cases} u_m, & M = 1,2,3, \\ \phi, & M = 4, \\ \Delta T, & M = 5, \end{cases} \tag{5}$$

where u_m is the elastic displacement, ϕ the electric potential and ΔT the temperature change with respect to a reference temperature. Thus one has

$$\begin{cases} \varepsilon_{ij} = \frac{1}{2}(u_{i,j} + u_{j,i}), \\ E_i = -\phi_{,i}, \\ e_i = -\Delta T_{,i}. \end{cases} \tag{6}$$

Recall that the quantities in the above shorthand notations are not tensors. Each individual tensor must be transformed by the well known laws of tensor transformations. Then, the resulting tensors can be reunified.

The topology of the present multi-coated inhomogeneity problem (see Fig. 1) consists of an inhomogeneity phase occupying a volume, V_1, whose behavior is described by the thermo-electro-elastic moduli pseudo-tensors $\mathbf{L}^1$ and $\boldsymbol{\beta}^1$. Surrounding this inhomogeneity phase are $(n-1)$ layers of coatings of other materials whose behaviors are described by their respective thermo-electro-elastic moduli pseudo-tensors $\mathbf{L}^i$ and $\boldsymbol{\beta}^i$ and that occupies a volume, $V_i, i \in \{2,3,\ldots,n\}$. Note that the coating n is a shell of the matrix material. This multi-coated inhomogeneity is then embedded in the effective material described by the unknown effective thermo-electro-elastic moduli pseudo-tensors $\mathbf{L}^{\text{eff}}$ and $\boldsymbol{\beta}^{\text{eff}}$. The following derivation is limited to the case of small perturbation theory and the interfaces matrix-coating, coating-coating and coating-inhomogeneity are assumed to be perfect, thus ensuring continuity of tension and displacements across these boundaries. Note that this kind of topology has been used for elastic composites [17] and viscoelastic composites [18].

2.2. Integral equation and localizations

Micromechanical schemes are based on two distinct steps: (i) localization, which determines the relationship between the microscopic (local) fields and the macroscopic (global) loading, and (ii) homogenization, which employs averaging techniques to

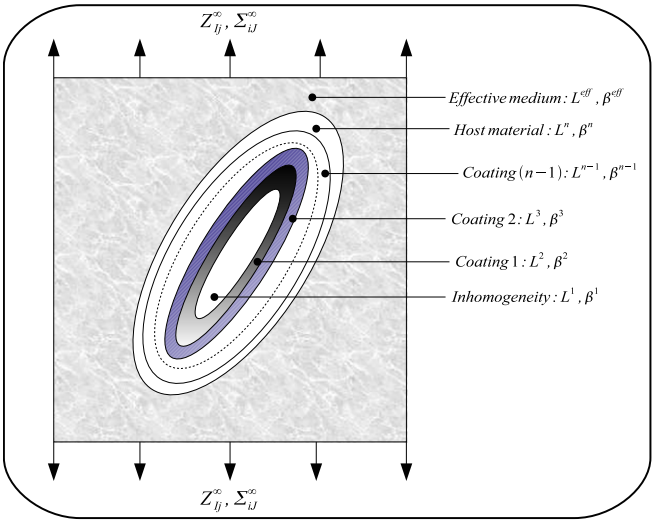

Fig. 1. Topology of the multi-coated inhomogeneity problem. Σ^{∞}_{ij} and Z^{∞}_{ij} represent the macroscopically applied fields.

approximate the macroscopic behavior. The beginning point of the present homogenization scheme is based on the integral equation of Zeller and Dederichs [24] who have proposed to model the composite material shown in Fig. 1 as a homogeneous material whose thermo-electro-elastic behavior varies spatially, that is

$$\begin{cases} \mathbf{L}(\mathbf{r}) = \mathbf{L}^{\text{eff}} + \delta\mathbf{L}(\mathbf{r}), \\ \boldsymbol{\beta}(\mathbf{r}) = \boldsymbol{\beta}^{\text{eff}} + \delta\boldsymbol{\beta}(\mathbf{r}), \end{cases} \tag{7}$$

where $\mathbf{r} \in V, V$ is the volume of the homogeneous medium, $\delta\mathbf{L}(\mathbf{r})$ and $\delta\boldsymbol{\beta}(\mathbf{r})$ are the spatially dependent thermo-electro-elastic moduli variations, $\mathbf{L}^{\text{eff}}$ and $\boldsymbol{\beta}^{\text{eff}}$ represent the unknown thermo-electro-elastic moduli of the effective material which are constant for all $\mathbf{r}$. To complete the formulation of the stationary linear response of a thermo-electro-elastic material, Eqs. (4) and (6) must be supplemented with the equations of the elastic equilibrium, the Gauss's law of electrostatics and the equation of heat conduction which in the absence of body forces, free charge and body heat sources are

$$\begin{cases} \sigma_{ij,i} = 0, \\ D_{i,i} = 0, \\ h_{i,i} = 0. \end{cases} \tag{8}$$

Based on the above shorthand notations, Eq. (8) gives

$$\Sigma_{iJ,i} = 0. \tag{9}$$

Using the symmetries of $\mathbf{C}, \mathbf{e}, \boldsymbol{\kappa}, \boldsymbol{k}, \boldsymbol{\sigma}$ and $\boldsymbol{\varepsilon}$, Eq. (9) yields

$$L^{\text{eff}}_{ijKl} U_{K,li} = [-\delta L_{ijKl} Z_{Kl} + \delta\beta_{ij}\Delta T]_{,i}. \tag{10}$$

Employing Green's formalism, one gets the simplified equation for the strain and the electrical fields, $Z_{Ij}(\mathbf{r})$, at any point in the medium as [25,24]

$$Z_{Ij}(\mathbf{r}) = Z^{\infty}_{Ij} - \int_V \Gamma^{\text{eff}}_{IjkL}(\mathbf{r}-\mathbf{r}')[\delta L_{kLMm}(\mathbf{r}')Z_{Mn}(r') - \delta\beta_{kL}(\mathbf{r})\Delta T]\mathrm{d}\mathbf{r}', \tag{11}$$

where $\boldsymbol{\Gamma}^{\text{eff}}(\mathbf{r}-\mathbf{r}')$ is the modified Green's thermo-electro-elastic pseudo-tensor, $\mathbf{Z}^{\infty}$ is the macroscopic elastic strain, heat strain and electric fields that have no spatial dependence. Here the superscript "eff" denotes that the Green's pseudo-tensor is computed using the thermo-electro-elastic properties, $\mathbf{L}^{\text{eff}}$, of the effective medium. The fluctuation parts of the thermo-electro-elastic constants with respect to the effective medium are given by the following relations

$$\begin{cases} \delta\mathbf{L}(\mathbf{r}) = \sum_{k=1}^{n} \Delta\mathbf{L}^{(k/\text{eff})}\theta_k(\mathbf{r}), \quad \text{with} \quad \Delta\mathbf{L}^{(k/\text{eff})} = (\mathbf{L}^k - \mathbf{L}^{\text{eff}}), \\ \delta\boldsymbol{\beta}(\mathbf{r}) = \sum_{k=1}^{n} \Delta\boldsymbol{\beta}^{(k/\text{eff})}\theta_k(\mathbf{r}), \quad \text{with} \quad \Delta\boldsymbol{\beta}^{(k/\text{eff})} = (\boldsymbol{\beta}^k - \boldsymbol{\beta}^{\text{eff}}), \end{cases} \tag{12}$$

where the characteristic function $\theta_k(\mathbf{r})$ of the phase k, occupying the volume V_k, is defined as

$$\theta_k(\mathbf{r}) = \begin{cases} 1 & \forall \mathbf{r} \in V_k \\ 0 & \forall \mathbf{r} \notin V_k \end{cases}, \quad \text{with } k \in \{0,1,2,\ldots,n\}. \tag{13}$$

For the following, certain notation conventions need to be mentioned. The volume V_{I} of the composite inhomogeneity, I, consists of the inhomogeneity and $(n-1)$ coatings and the volume fraction, φ_k, of the phase k are defined as

$$V_{\text{I}} = \sum_{k=1}^{n} V_k \quad \text{and} \quad \varphi_k = \frac{V_k}{V_{\text{I}}}, \quad k \in \{1,2,\ldots,n\}. \tag{14}$$

The average strain and electrical fields, $\overline{\mathbf{Z}}^{\text{I}}$, in the composite inhomogeneity, I, is defined by

$$\overline{\mathbf{Z}}^{\text{I}} = \frac{1}{V_{\text{I}}}\int_{V_{\text{I}}} \mathbf{Z}(\mathbf{r})\mathrm{d}\mathbf{r} = \mathbf{Z}^{\infty} - \mathbf{T}^{\text{I}}(\mathbf{L}^{\text{eff}}) : \boldsymbol{\tau}^{\text{I}}, \tag{15}$$

where

$$\begin{cases} \mathbf{T}^{\text{I}}(\mathbf{L}^{\text{eff}}) = \frac{1}{V_{\text{I}}}\int_{V_{\text{I}}}\int_{V_{\text{I}}} \boldsymbol{\Gamma}^{\text{eff}}(\mathbf{r}-\mathbf{r}')\mathrm{d}\mathbf{r}\mathrm{d}\mathbf{r}', \\ \boldsymbol{\tau}^{\text{I}} = \sum_{k=1}^{n} \varphi_k\left(\Delta\mathbf{L}^{(k/\text{eff})} : \overline{\mathbf{Z}}^k - \Delta\boldsymbol{\beta}^{(k/\text{eff})}\Delta T\right), \\ \overline{\mathbf{Z}}^k = \frac{1}{V_k}\int_{V_k} \mathbf{Z}(\mathbf{r})\mathrm{d}\mathbf{r}. \end{cases} \tag{16}$$

It is obvious from Eq. (15) that if one can find the local concentration pseudo-tensors, $\mathbf{a}^k$ and $\mathbf{b}^k$, such that

$$\overline{\mathbf{Z}}^k = \mathbf{a}^k : \overline{\mathbf{Z}}^{\text{I}} + \mathbf{b}^k\Delta T, \tag{17}$$

then, the localization pseudo-tensors, $\mathbf{A}^{\text{I}}$ and $\mathbf{B}^{\text{I}}$, in the composite inhomogeneity, I, which are defined by the relation

$$\overline{\mathbf{Z}}^{\text{I}} = \mathbf{A}^{\text{I}} : \overline{\mathbf{Z}}^{\infty} + \mathbf{B}^{\text{I}}\Delta T, \tag{18}$$

can be determined as

$$\begin{cases} \mathbf{A}^{\text{I}} = \left[\mathbf{I}^4 + \mathbf{T}^{\text{I}}(\mathbf{L}^{\text{eff}}) : \left(\sum_{k=1}^{n} \varphi_k\Delta\mathbf{L}^{(k/\text{eff})} : \mathbf{a}^k\right)\right]^{-1}, \\ \mathbf{B}^{\text{I}} = -\mathbf{A}^{\text{I}} : \mathbf{T}^{\text{I}}(\mathbf{L}^{\text{eff}}) : \left[\sum_{k=1}^{n} \varphi_k(\Delta\mathbf{L}^{(k/\text{eff})} : \mathbf{b}^k - \Delta\boldsymbol{\beta}^{(k/\text{eff})})\right]. \end{cases} \tag{19}$$

In Eq. (19), $\mathbf{I}^4$ is the shorthand notation for the fourth order and the second order identity tensors, i.e.

$$I^4_{IjMn} = \begin{cases} (\delta_{im}\delta_{jn} + \delta_{in}\delta_{jm}), & I,M = 1,2,3, \\ 0, & I = 1,2,3;\ M = 4,5, \\ 0, & M = 1,2,3;\ I = 4,5, \\ \delta_{jn}, & I = M = 4, \\ \delta_{jn}, & I = M = 5, \end{cases} \tag{20}$$

where δ_{ij} is the Kronecker delta. To complete the localization step, the local localization pseudo-tensors, $\mathbf{a}^k$ and $\mathbf{b}^k$, must be found. If one introduces the localization pseudo-tensors, $\mathbf{A}^k$ and $\mathbf{B}^k$, in each phase, k, such as

$$\overline{\mathbf{Z}}^k = \mathbf{A}^k : \mathbf{Z}^{\infty} + \mathbf{B}^k\Delta T, \tag{21}$$

then, Eqs. (17) and (18) give

$$\begin{cases} \mathbf{A}^k = \mathbf{a}^k : \mathbf{A}^{\text{I}}, \\ \mathbf{B}^k = \mathbf{a}^k : \mathbf{B}^{\text{I}} + \mathbf{b}^k. \end{cases} \tag{22}$$

Using the fact that

$$\overline{\mathbf{Z}}^{\mathrm{I}} = \langle \overline{\mathbf{Z}}^{k} \rangle = \sum_{k=1}^{n} \varphi_k \overline{\mathbf{Z}}^{k}, \tag{23}$$

one gets the following equations to solve for $\mathbf{a}^k$ and $\mathbf{b}^k$

$$\begin{cases} \langle \mathbf{a}^k \rangle = \sum\limits_{k=1}^{n} \varphi_k \mathbf{a}^k = \mathbf{I}^4, \\ \langle \mathbf{b}^k \rangle = \sum\limits_{k=1}^{n} \varphi_k \mathbf{b}^k = 0. \end{cases} \tag{24}$$

Here, the notation, $\langle \zeta \rangle$, denotes the average value of the quantity, ζ, over the whole volume of the composite inhomogeneity, I. Eqs. (24) constitute the solution of the posed problem given as function of the unknown n local localization pseudo-tensors, $\mathbf{a}^k$ and $\mathbf{b}^k$, which can be determined if one takes into account the boundary conditions through the different interfaces in the composite inhomogeneity. Interfacial operators [26] are a very convenient mathematical tool that efficiently calculates the stress or strain jump across a material interface (an interface separating two dissimilar materials). These operators are derived by writing the equations for the continuity of displacement and tension across the material interface (hypothesis of perfect interface). The derivation begins with the general case of two solid phases k and $(k+1)$, with the thermo-electro-elastic constants $\mathbf{L}^k, \boldsymbol{\beta}^k, \mathbf{L}^{k+1}$ and $\boldsymbol{\beta}^{k+1}$ separated by a surface with unit normal, $\mathbf{N}$, directed from phase k to phase $(k+1)$. Using the thermo-electro-elastic constants of these two phases, the jump of $\mathbf{Z}(\mathbf{r})$ across the material interface is given as follows [26]

$$Z_{Ij}^{k+1}(\mathbf{r}) - Z_{Ij}^{k}(\mathbf{r}) = P_{IjmN}^{k+1}\left[\left(L_{mNPq}^{k} - L_{mNPq}^{k+1}\right) Z_{Pq}^{k}(\mathbf{r}) + \left(\beta_{mN}^{k} - \beta_{mN}^{k+1}\right)\Delta T\right]. \tag{25}$$

The interfacial operator, P_{IjmN}^{k+1}, depends only on the constituent materials's properties and the unit normal vector of the interface. In the following, some notation conventions need to be defined

$$\Omega_j = \bigcup_{k=1}^{j} V_k \quad \text{and} \quad \Delta\mathbf{L}^{(p/q)} = \mathbf{L}^{p} - \mathbf{L}^{q}. \tag{26}$$

Substituting $\mathbf{Z}^k(\mathbf{r})$ by the average value, $\overline{\mathbf{Z}}^{\Omega_k}$, of $\mathbf{Z}(\mathbf{r})$ over the volume Ω_k and taking the average, $\overline{\mathbf{Z}}^{k+1}$, of $\mathbf{Z}(\mathbf{r})$ over the volume V_{k+1}, Eq. (25) yields

$$\overline{\mathbf{Z}}^{k+1} = \overline{\mathbf{Z}}^{\Omega_k} + \mathbf{T}^{k+1}(\mathbf{L}^{k+1}) : [\Delta\mathbf{L}^{(\Omega_k/k+1)} : \overline{\mathbf{Z}}^{\Omega_k} + \Delta\boldsymbol{\beta}^{(\Omega_k/k+1)}\Delta T], \tag{27}$$

where $\mathbf{L}^{\Omega_k}$ and $\boldsymbol{\beta}^{\Omega_k}$ are the thermo-electro-elastic moduli of the composite formed by the volume Ω_k,

$$\mathbf{T}^{k+1}(\mathbf{L}^{k+1}) = \frac{1}{V_{k+1}} \int_{V_{k+1}} \mathbf{P}^{k+1} \mathrm{d}\mathbf{r}, \tag{28}$$

and

$$\overline{\mathbf{Z}}^{\Omega_k} = \sum_{i=1}^{k} \frac{V_i}{\Omega_k} \overline{\mathbf{Z}}^{i} = \frac{\sum_{i=1}^{k} \varphi_i \overline{\mathbf{Z}}^{i}}{\sum_{i=1}^{k} \varphi_i}. \tag{29}$$

Following [27], it can be shown that

$$\mathbf{T}^{k+1}(\mathbf{L}^{k+1}) = \mathbf{T}^{\Omega_k}(\mathbf{L}^{k+1}) - \frac{\sum_{i=1}^{k} \varphi_i}{\varphi_{k+1}} [\mathbf{T}^{\Omega_{k+1}}(\mathbf{L}^{k+1}) - \mathbf{T}^{\Omega_k}(\mathbf{L}^{k+1})], \tag{30}$$

with

$$\mathbf{T}^{\Omega_p}(\mathbf{L}^{q}) = \frac{1}{\Omega_p} \int_{\Omega_p} \int_{\Omega_p} \boldsymbol{\Gamma}(\mathbf{L}^{q})(\mathbf{r} - \mathbf{r}') \mathrm{d}\mathbf{r} \mathrm{d}\mathbf{r}'. \tag{31}$$

Since $\mathbf{T}^{\Omega_p}(\mathbf{L}^q)$ are not size-dependent but shape dependent, it is obvious that in the specific case of homothetic inhomogeneities, one has

$$\mathbf{T}^{k+1}(\mathbf{L}^{k+1}) = \mathbf{T}^{\Omega_k}(\mathbf{L}^{k+1}) = \mathbf{T}^{\Omega_{k+1}}(\mathbf{L}^{k+1}). \tag{32}$$

Using some algebraic manipulations, one gets

$$\Delta\mathbf{L}^{(\Omega_k/k+1)} : \overline{\mathbf{Z}}^{\Omega_k} + \Delta\boldsymbol{\beta}^{(\Omega_k/k+1)}\Delta T = \frac{\sum_{j=1}^{k} \varphi_j (\Delta\mathbf{L}^{(j/k+1)} : \overline{\mathbf{Z}}^{j} + \Delta\boldsymbol{\beta}^{(j/k+1)}\Delta T)}{\sum_{j=1}^{k} \varphi_j}. \tag{33}$$

If one introduces the pseudo-tensors $\boldsymbol{\Pi}^k$ and $\boldsymbol{\Delta}^k$ defined by

$$\begin{cases} \mathbf{a}^k = \boldsymbol{\Pi}^k : \mathbf{a}^1, \\ \mathbf{b}^k = \boldsymbol{\Pi}^k : \mathbf{b}^1 + \boldsymbol{\Delta}^k, \end{cases} \tag{34}$$

then, by using Eqs. (27), (29) and (33), the pseudo-tensors $\boldsymbol{\Pi}^k$ and $\boldsymbol{\Delta}^k$ are obtained as follows

$$\begin{cases} \boldsymbol{\Pi}^k = \frac{\sum_{j=1}^{k-1} (\varphi_j \boldsymbol{\vartheta}^{(j/k)} : \boldsymbol{\Pi}^j)}{\sum_{j=1}^{k-1} \varphi_j}, \\ \boldsymbol{\Delta}^k = \frac{\sum_{j=1}^{k-1} \varphi_j (\boldsymbol{\vartheta}^{(j/k)} : \boldsymbol{\Delta}^j + \boldsymbol{\chi}^{(j/k)})}{\sum_{j=1}^{k-1} \varphi_j}. \end{cases} \tag{35}$$

In Eq. (35), the expressions of the pseudo-tensors $\boldsymbol{\vartheta}^{(j/k)}$ and $\boldsymbol{\chi}^{(j/k)}$ are given as

$$\begin{cases} \boldsymbol{\vartheta}^{(j/k)} = \mathbf{I}^4 + \mathbf{T}^k(\mathbf{L}^k) : \Delta\mathbf{L}^{(j/k)}, \\ \boldsymbol{\chi}^{(j/k)} = \mathbf{T}^k(\mathbf{L}^k) : \Delta\boldsymbol{\beta}^{(j/k)}. \end{cases} \tag{36}$$

One can verify that

$$\boldsymbol{\Pi}^1 = \mathbf{I}^4, \quad \text{and} \quad \boldsymbol{\Delta}^1 = 0. \tag{37}$$

Furthermore, Eqs. (24) and (34) give finally

$$\begin{cases} \mathbf{a}^1 = \left(\sum\limits_{k=1}^{n} \varphi_k \boldsymbol{\Pi}^k\right)^{-1}, \\ \mathbf{b}^1 = -\mathbf{a}^1 : \left(um_{k=1}^{n} \varphi_k \boldsymbol{\Delta}^k\right). \end{cases} \tag{38}$$

The localization step of the present micromechanical model is definitively complete once the pseudo-tensors $\mathbf{a}^1$ and $\mathbf{b}^1$ are known.

2.3. Summary of the localization step

To sum up, the main objective of the Section 2.2 is to compute the localization pseudo-tensors $\mathbf{A}^k$ and $\mathbf{B}^k$ defined by the formula (21). The steps to get $\mathbf{A}^k$ and $\mathbf{B}^k$ are as follows

- from the properties $\mathbf{L}^k$ of each phase, compute $\mathbf{T}^k(\mathbf{L}^k)$ using Eq. (30);
- compute $\boldsymbol{\vartheta}^{(j/k)}$ and $\boldsymbol{\chi}^{(j/k)}$ from Eq. (36) using the properties $\boldsymbol{\beta}^k$;
- compute $\boldsymbol{\Pi}^k$ and $\boldsymbol{\Delta}^k$ from Eqs. (35) and (37);
- compute $\mathbf{a}^1$ and $\mathbf{b}^1$ from Eq. (38) and get $\mathbf{a}^k$ and $\mathbf{b}^k$ from Eq. (34);
- compute $\mathbf{A}^1$ and $\mathbf{B}^1$ from Eq. (19) and finally get $\mathbf{A}^k$ and $\mathbf{B}^k$ from Eq. (22).

2.4. Homogenization schemes and effective properties

In what follows, two approaches are presented to compute the effective properties of a piezoelectric material containing ellipsoidal shaped multi-coated inhomogeneities. Both approaches are based on the classical self-consistent scheme. The first scheme is the basis of the second one that uses it in an incremental way. The second approach has been shown very useful in the case of high volume fractions of inhomogeneities with high contrast between the properties of the host material and the inhomogeneities.

2.4.1. Non-incremental homogenization scheme

The effective thermo-electro-elastic properties $\mathbf{L}^{\mathrm{eff}}$ and $\boldsymbol{\beta}^{\mathrm{eff}}$ are related to the macroscopic fields $\boldsymbol{\Sigma}^{\infty}$ and $\mathbf{Z}^{\infty}$ as

$$\boldsymbol{\Sigma}^{\infty} = \mathbf{L}^{\text{eff}} : \mathbf{Z}^{\infty} - \boldsymbol{\beta}^{\text{eff}} \Delta T. \tag{39}$$

Using the following relations

$$\begin{cases} \boldsymbol{\Sigma}^{\infty} = \sum_{k=0}^{n} \varphi_k \overline{\boldsymbol{\Sigma}}^k, \\ \mathbf{Z}^{\infty} = \sum_{k=0}^{n} \varphi_k \overline{\mathbf{Z}}^k, \\ \overline{\boldsymbol{\Sigma}}^k = \mathbf{L}^k : \overline{\mathbf{Z}}^k - \boldsymbol{\beta}^k \Delta T, \end{cases} \tag{40}$$

in Eq. (39), one gets

$$\begin{cases} \mathbf{L}^{\text{eff}} = \sum_{k=0}^{n} \varphi_k \mathbf{L}^k : \mathbf{A}^k, \\ \boldsymbol{\beta}^{\text{eff}} = \sum_{k=0}^{n} \varphi_k (\boldsymbol{\beta}^k - \mathbf{L}^k : \mathbf{B}^k). \end{cases} \tag{41}$$

Eq. (41) is a set of nonlinear equations (since the localization pseudo-tensors, $\mathbf{A}^k$ and $\mathbf{B}^k$ are functions of $\mathbf{L}^{\text{eff}}$ and $\boldsymbol{\beta}^{\text{eff}}$) to solve for the effective properties $\mathbf{L}^{\text{eff}}$ and $\boldsymbol{\beta}^{\text{eff}}$. The localization pseudo-tensors, $\mathbf{A}^k$ and $\mathbf{B}^k$ are all determined in the localization step (Section 2.2). This non-incremental homogenization scheme is called herein the generalized self-consistent method (GSCM). The implementation of this micromechanical modeling technique requires the numerical approximation of the integral of the modified Green's thermo-electro-elastic pseudo-tensor $\boldsymbol{\Gamma}(\mathbf{L}^X)$ needed to compute $\mathbf{T}^{\text{I}}(\mathbf{L}^{\text{eff}})$ (see Eq. (19)) and $\mathbf{T}^{\Omega_p}(\mathbf{L}^q)$ (see Eq. (30)). The implementation details of theses pseudo-tensors can be found in the appendix B of [9]. Note that, $\mathbf{T}^{\Omega_p}(\mathbf{L}^q)$ can be also obtained from the Eshelby's thermo-electro-elastic pseudo-tensor, $\mathbf{S}^{\Omega_p}(\mathbf{L}^q)$, as

$$\mathbf{T}^{\Omega_p}(\mathbf{L}^q) = \mathbf{S}^{\Omega_p}(\mathbf{L}^q) : (\mathbf{L}^q)^{-1}. \tag{42}$$

Expressions for the components of $\mathbf{S}^{\Omega_p}(\mathbf{L}^q)$ can be found in [28,29].

2.4.2. Incremental homogenization scheme

It has been noticed that the classical self-consistent method (CSCM) poorly estimates the effective properties of composites at high concentrations of reinforcements and is limited to very low concentrations for composite materials containing voids [8] or composites with high contrast between the properties of the matrix and the inhomogeneities. In order to avoid this drawback, an improvement of the CSCM has been proposed in [30] for the elastic case, which gives a progressive construction of the composite material in an incremental way in the same manner as the differential scheme (DS). In this paper, this incremental method is extended to the thermo-electro-elastic behavior of piezoelectric composite materials. In the incremental scheme, the construction of the material is made by placing a finite increments of the volume fractions of the inhomogeneities in a certain effective medium, and for each increment the GSCM is applied to calculate the effective thermo-electro-elastic properties of the piezoelectric composite material. If S is the number of steps to use, the expression of the volume fraction increment, $\Delta\varphi_k^i$, of the k^{th} inhomogeneity phase at the i^{th} step is given as [30]

$$\Delta\varphi_k^i = \frac{\Delta\varphi_k}{1 - (i-1)\sum_{j=1}^{n-1} \Delta\varphi_j}, \quad k \in \{1, 2, \ldots, n-1\}, \tag{43}$$

where

$$\Delta\varphi_k = \frac{\varphi_k}{S}. \tag{44}$$

At the i^{th} step, the matrix phase becomes the effective material obtained at the $(i\text{-}1)^{\text{th}}$ step using the GSCM with the volume fractions $\Delta\varphi_k^{i-1}$. This incremental scheme is referred as IGSCM hereafter. Recall that this incremental scheme does not affect the expression of the concentration pseudo-tensors $\mathbf{A}^k$ and $\mathbf{B}^k$ on which the method is based. So, the formulation used in this case is the same as in the GSCM. The two methods differ only in the manner of introducing the reinforcements volume fractions.

3. Finite element modelization

A finite element analysis (FEA) of the representative volume element (RVE) is performed to verify the results obtained from the micromechanical models presented in Section 2. It consists of a cube containing an ellipsoidal inhomogeneity (see Fig. 2). The number of elements in the RVE varies from 1000 to 1500, depending on the volume fraction of the inhomogeneities. A convergence study is always carried out to determine the appropriate number of elements to be used for each case. For geometrical reasons the volume fraction of the inhomogeneity can't rise up to the unity. In the case of spherical inclusion, the theoretical limit is 0.523, whereas in this work it is limited to 0.45 to avoid meshing problems. The computation of the effective properties is based on the numerical approach developed in [19] for the electro-mechanical properties and in [20] for the temperature stress coefficients. The pyroelectric constants can't be evaluated because of the lack of appropriate finite elements, whereas for the thermal conductivity constants a specific approach is developed.

Rigorously, the boundary conditions should be applied on the surface of the RVE point wise in order to guarantee the periodicity condition. However, for this kind of problem, it is sufficient to apply uniform boundary condition on the faces of the cubic RVE. If (x_1, x_2, x_3) denotes an orthogonal reference system whose axes are perpendicular to the faces of the cubic RVE, the appropriate boundary conditions can be expressed more easily naming A^- and A^+ the faces perpendicular to direction x_1, B^- and B^+ the faces perpendicular to direction x_2, C^- and C^+ the faces perpendicular to direction x_3. For the electro-mechanical properties, six different load cases with the corresponding computed properties, in the case of transversal isotropic materials, are shown in Table 1, where q is an arbitrary quantity, u are the displacements and ϕ is the electric potential. The finite elements used to evaluate the electro-mechanical properties are standard ABAQUS's 8-node linear piezoelectric

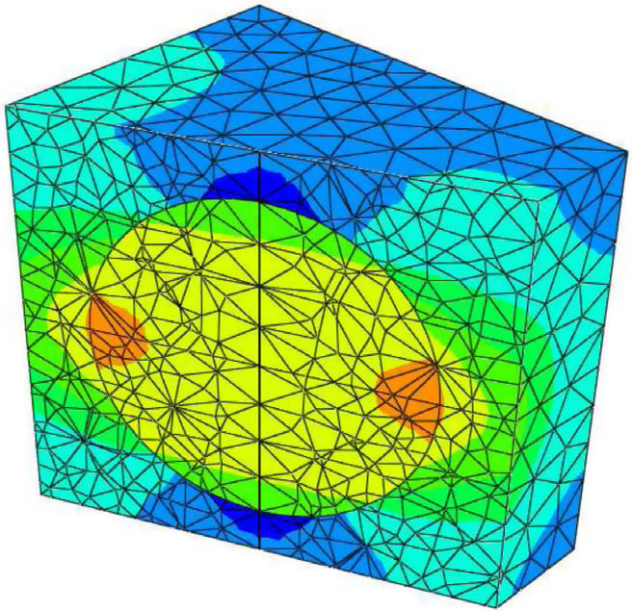

Fig. 2. Finite element modeling of the RVE, cut with a skew plane. In colors, stress distribution σ_{11} corresponding to a particular load case for the evaluation of the components of the elastic moduli tensor.

Table 1
Periodic boundary conditions for different load cases.

Case	Mechanical and electrical BC			Properties
	A faces	B faces	C faces	
1	$u_{1A^+}=q$ and $u_{1A^-}=0$ $\phi_{A^+}=0$ and $\phi_{A^-}=0$	$u_{2B^+}=0$ and $u_{2B^-}=0$ $\phi_{B^+}=0$ and $\phi_{B^-}=0$	$u_{3C^+}=0$ and $u_{3C^-}=0$ $\phi_{C^+}=0$ and $\phi_{C^-}=0$	C^E_{11}, C^E_{21}
2	$u_{1A^+}=0$ and $u_{1A^-}=0$ $\phi_{A^+}=0$ and $\phi_{A^-}=0$	$u_{2B^+}=0$ and $u_{2B^-}=0$ $\phi_{B^+}=0$ and $\phi_{B^-}=0$	$u_{3C^+}=q$ and $u_{3C^-}=0$ $\phi_{C^+}=0$ and $\phi_{C^-}=0$	C^E_{13}, C^E_{33}
3	$u_{1A^+}=0$ and $u_{1A^-}=0$ $\phi_{A^+}=0$ and $\phi_{A^-}=0$	$u_{3B^+}=q$ and $u_{3B^-}=0$ $\phi_{B^+}=0$ and $\phi_{B^-}=0$	$u_{2C^+}=q$ and $u_{2C^-}=0$ $\phi_{C^+}=0$ and $\phi_{C^-}=0$	C^E_{44}, e_{24}
4	$u_{2A^+}=q$ and $u_{2A^-}=0$ $\phi_{A^+}=0$ and $\phi_{A^-}=0$	$u_{1B^+}=q$ and $u_{1B^-}=0$ $\phi_{B^+}=0$ and $\phi_{B^-}=0$	$u_{3C^+}=0$ and $u_{3C^-}=0$ $\phi_{C^+}=0$ and $\phi_{C^-}=0$	C^E_{66}
5	$u_{1A^+}=0$ and $u_{1A^-}=0$ $\phi_{A^+}=0$ and $\phi_{A^-}=0$	$u_{2B^+}=0$ and $u_{2B^-}=0$ $\phi_{B^+}=0$ and $\phi_{B^-}=0$	$u_{3C^+}=0$ and $u_{3C^-}=0$ $\phi_{C^+}=q$ and $\phi_{C^-}=0$	$\kappa^{\varepsilon}_{33}, e_{31}, e_{33}$
6	$u_{1A^+}=0$ and $u_{1A^-}=0$ $\phi_{A^+}=q$ and $\phi_{A^-}=0$	$u_{2B^+}=0$ and $u_{2B^-}=0$ $\phi_{B^+}=0$ and $\phi_{B^-}=0$	$u_{3C^+}=0$ and $u_{3C^-}=0$ $\phi_{C^+}=0$ and $\phi_{C^-}=0$	$\kappa^{\varepsilon}_{11}$

Table 2
Electro-elastic material properties. C_{ij} in GPa, e_{ij} in C m^{-2}, $\kappa_0 = 8.854\times10^{-12}$ C N^{-1} m^{-2}.

	C_{11}	C_{12}	C_{13}	C_{33}	C_{44}	e_{31}	e_{33}	e_{15}	κ_{11}/κ_0	κ_{33}/κ_0
Epoxy	8	4.4	4.4	8	1.8	0	0	0	4.2	4.2
$BaTiO_3$	150	66	66	146	4.4	−4.3	17.5	11.4	1115	1260
PZT-4	139	77.8	74.3	115	25.6	−5.2	15.1	12.7	730	645
PZT-5	121	75.4	75.2	111	21.1	−5.4	15.8	12.3	916	830
PZT-7A	148	76.2	74.2	131	25.4	−2.1	12.3	9.2	460	235

brick elements (C3D8E). Differently from the work in [19], all the mechanical boundary conditions are expressed in terms of the displacements, not in terms of both displacements and loads.

To evaluate the temperature stress coefficients and the thermal conductivity constants, the standard ABAQUS thermo-elastic 8-node thermally coupled brick, trilinear displacement and temperature (C3D8T) are used. Details for the evaluation of the temperature stress coefficients can be found in [20]. The evaluation of the thermal conductivity constants required the development of a specific approach. The difficulty consists in the calculation of the heat strain vector averaged over the whole RVE. In fact, the heat strain vector is not an output in many commercial finite element codes. The solution proposed here is to apply to a face of the RVE a prescribed uniform temperature and to the opposite face the same uniform temperature increased of one degree. In this way, it can be assumed that the averaged heat strain vector has the component along the direction normal to these faces equal to one divided by the length of the cubic edge, while the other two components are null. All the displacements on the faces of the RVE have to be set to zero. This approach can be proved to be valid because of the symmetries of the problem and the results obtained are validated with experimental data.

4. Numerical results and discussions

The effective properties of a polymeric matrix containing piezoelectric material inhomogeneities are evaluated with the proposed micromechanical models and with the finite element analysis. The electro-elastic properties of the constituent materials are shown in Table 2, whereas the thermal properties are given in Table 3. In what follows, the inhomogeneity semi-axis along the x_1, x_2 and x_3 directions will be denoted a, b and c respectively. The special case of $a = b$ will be considered. The matrix is made of Epoxy material while the inhomogeneity is made of one of the piezoelectric materials ($BaTiO_3$, PZT-4, PZT-4 or PZT-7A) in Table 2. The polarization direction is assumed to be x_3 direction if not otherwise specified.

Table 3
Thermal material properties. α_{ij} in $(\times10^{-6})$ K^{-1}, p_i in V m^{-1} K^{-1}, k in W m^{-1} K^{-1}.

	α_{11}	α_{33}	p_3	k
Epoxy	60	60	0	0.7
$BaTiO_3$	8.53	1.99	13,300	2.9
PZT-5	8.53	1.99	13,300	1.1

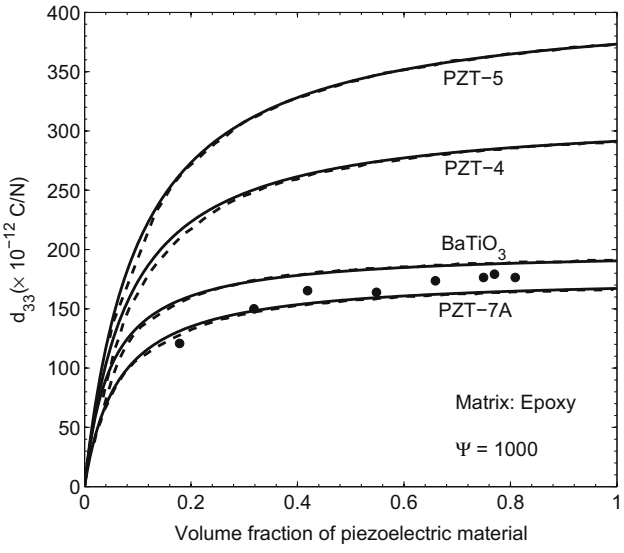

Fig. 3. Effective d_{33} calculated with inclusion of different materials. Incremental scheme in solid lines (-), non-incremental scheme in dashed lines (- -), experimental results from [21] in dots (•).

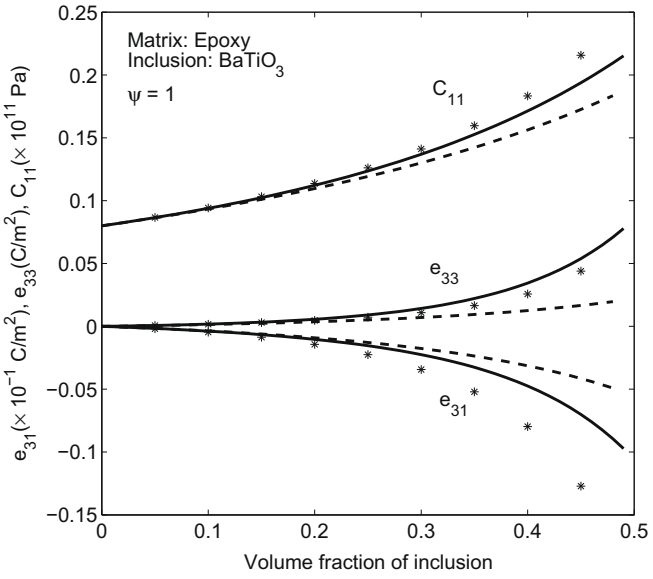

Fig. 4. Comparison between incremental scheme (solid lines -), non-incremental scheme (dashed lines - -) and FEA results (asterisks $*$).

Results obtained with the micromechanical models in the case of fiber shape inhomogeneity (aspect ratio $c/a = \Psi = 1000$) are shown in Fig. 3. The results for PZT-7A are in good agreement with the experimental data found in [21]. For this particular geometry there is no significant difference between the results obtained with the incremental (solid lines) and the non-incremental (dashed lined) schemes. This is not the case if the inhomogeneity has a spherical shape ($\Psi = 1$), see Fig. 4.

The results obtained with the micromechanical models are plotted together with the results from the finite element homogenization up to the volume fraction of 0.5. The effective properties obtained from the incremental scheme are higher than the ones given by the non-incremental scheme for all the considered properties. This difference increases with the volume fraction of the inhomogeneities and it is more pronounced above the volume fraction of 0.2. Table 4 reports a comparison between the results shown in Fig. 4 for different volume fractions. The results obtained from the FEM homogenization are in better agreement with the incremental scheme rather than with the non-incremental scheme. Moreover the non-piezoelectric properties predicted by the micromechanical model are closer than the piezoelectric properties to the FEM homogenization results. It is important to notice that, the effective piezoelectric coefficients are very small with respect to the ones of the piezoelectric constituent material. The reason of this behavior is the great mismatch between the dielectric coefficients, κ^c_{ij}, of the matrix and the inclusion materials. For a matrix material having dielectric coefficients similar to that of the inhomogeneity, the predicted piezoelectric coefficients are much larger.

In Fig. 5, the thermal conductivity calculated with the micromechanical models and the FEM homogenization is compared to the experimental data from [22] for spherical alumina inhomogeneities ($k = 29$) in a glass matrix ($k = 1.4$).

There is a good agreement between the experimental data and the FEM homogenization results, both lying in between the results of the non-incremental method and the ones of the incremental method.

The influence of the aspect ratio on the effective properties computed with the micromechanical models is shown in Fig. 6.

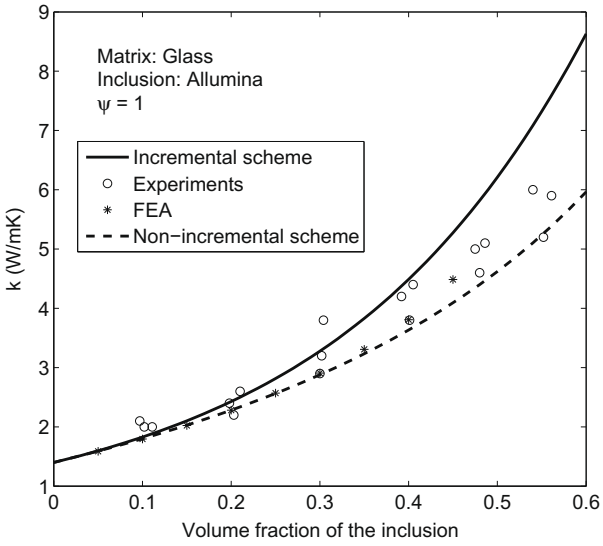

Fig. 5. Comparison between incremental scheme (solid lines -), non-incremental scheme (dashed lines - -), FEA results (asterisks $*$) and experimental results from [22] (circles $\circ$) for the thermal conductivity.

Table 4
Comparison between results obtained with the FEM homogenization, the non-incremental scheme (NI) and the incremental scheme (I). The differences between the results of the micromechanical models and that of the FEM homogenization are reported in percentage. C_{11} in $(\times 10^{10})$Pa, e_{31} in $(\times 10^{-3})$ C m^{-2}, e_{33} in $(\times 10^{-2})$ C m^{-2}, α_{33} in $(\times 10^{-5})$ K^{-1}. Matrix: Epoxy. Inclusion: $BaTiO_3$ $\Psi = 1$.

Volume fraction	Property	FEM	NI	I	err(NI)	err(I)
0.1	C_{11}	0.942	0.933	0.939	−0.94	−0.33
	e_{31}	−0.465	−0.363	−0.381	−22.0	−18.1
	e_{33}	0.166	0.145	0.177	−12.7	6.21
	α_{33}	5.17	5.29	5.26	2.34	1.67
0.2	C_{11}	1.14	1.10	1.12	−3.54	−1.27
	e_{31}	−1.44	−0.909	−1.03	−36.7	−28.0
	e_{33}	0.475	0.364	0.562	−23.5	18.3
	α_{33}	4.40	4.80	4.56	6.27	3.63
0.3	C_{11}	1.41	1.30	1.37	−7.87	−2.98
	e_{31}	−3.44	−1.75	−2.24	−48.9	−34.6
	e_{33}	1.09	0.703	1.42	−35.5	30.6
	α_{33}	3.69	4.12	3.88	11.6	5.34
0.4	C_{11}	1.83	1.56	1.71	−14.7	−6.51
	e_{31}	−7.97	−3.13	−4.74	−60.7	−40.4
	e_{33}	2.57	1.25	3.44	−51.3	33.7
	α_{33}	2.99	3.58	3.21	19.7	7.37

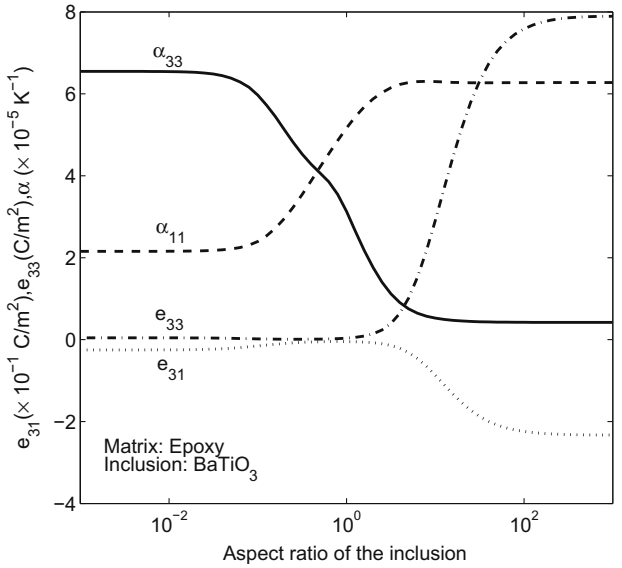

Fig. 6. Effect of the aspect ratio of the inclusion on the effective properties. The volume fraction of inclusion is 0.4.

The volume fraction is fixed at 0.4. With $\Psi < 10^{-1}$ and with $\Psi > 10^{2}$ the effective properties do not have significant variations and have an asymptotic behavior. This means that, for this model, $\Psi = 10^{-1}$ is a good approximation of a penny-shaped inclusion while $\Psi = 10^{2}$ is a good approximation of a fiber-like inclusion. The two thermal expansion coefficients vary in an opposite way with each other: the influence of the inclusion on α_{11} is greater with penny-shaped inclusion whereas the influence on α_{33} is greater with fiber-like inclusion. The two thermal expansion coefficients lines cross each other for an inclusion that is not spherical, because the properties of the inclusion are not isotropic.

The effect of the rotation of the polarization direction with respect to the x_3 axis for an inclusion with $\Psi = 10$ and a volume fraction of 0.4 is shown in Fig. 7. When the polarization direction is perpendicular to the x_3 direction, the piezoelectric properties e_{31} and e_{33} are correctly null.

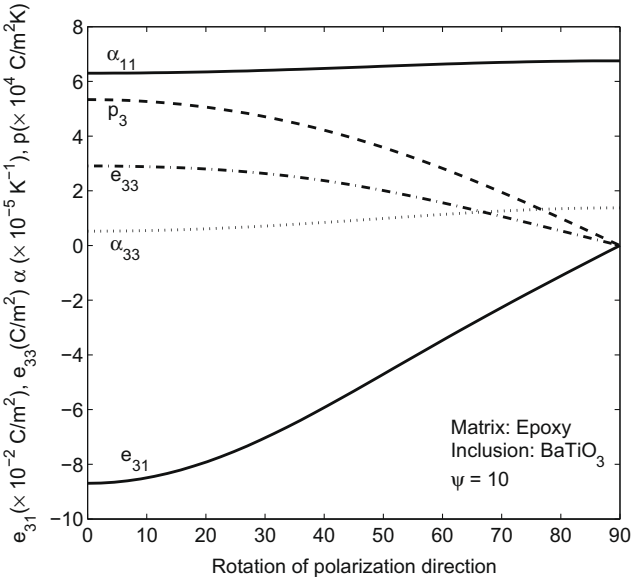

Fig. 7. Effect of the rotation of the polarization of the inclusion with respect to the x_3 axis on the effective properties. The volume fraction of inclusion is 0.4.

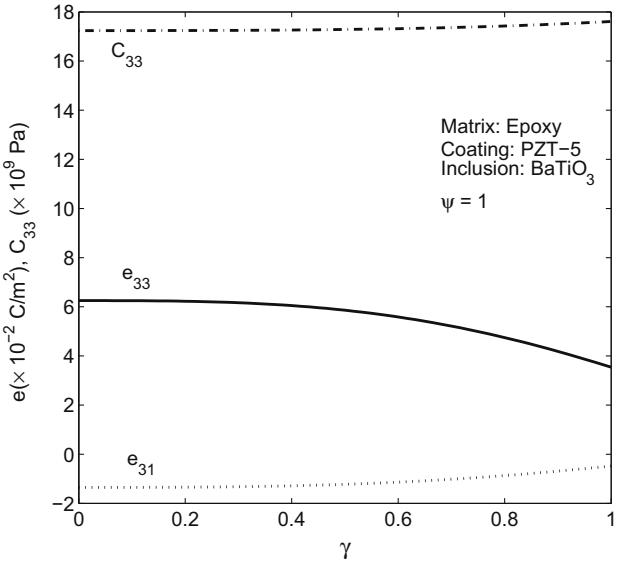

Fig. 8. Effect of the variation of the coating thickness with volume fraction of matrix fixed at 0.6.

The effect of a spherical coating in PZT-4 on a spherical inclusion in $BaTiO_3$ is shown in Fig. 8, where $\gamma = a_1/a_2 = b_1/b_2 = c_1/c_2$, as it is defined in [31] (the subscript 1 stands for the inclusion and 2 stands for the coating). The volume fraction of the matrix is fixed at 0.6.

5. Conclusion

In this paper a micromechanics-based model is proposed to predict the effective thermo-electro-elastic properties of piezoelectric composite materials containing multi-coated inhomogeneities. It is based on the generalized self consistent incremental scheme in which the composite inclusion has an ellipsoidal shape and the number of coatings is a free parameter. The incremental approach assures a better prediction of the effective properties in case of great difference among the properties of the constituent material, in particular for high volume fractions. The multi-coating formulation has the potential to study the effect of non-trivial inclusions, such as the ones made of functionally graded materials. The results obtained with the micro-mechanical model are in good agreement with experimental data and with the results obtained from a FEM homogenization. More results regarding the effect of the shape of the inclusion, the rotation of the poling direction and the presence of a coating are presented. The model proposed here has a wide range of applications thanks to its multi-coating capability and thanks to the wide set of properties considered. Moreover it can be easily extended in order to take into account other properties, like the magnetic ones. Further work may address design issues like problems of optimization of the characteristics of the inclusion to match the desired effective properties for materials by design issues.

Acknowledgements

This work has been developed in the context of the FNR MAFICOMECH Project (C08/MS/17). The authors acknowledge the financial support of the FNR via the AFR Grants (PHD-08-069, BFR08/071).

References

[1] Smith WA, Shauov A. Tailoring the properties of composite piezoelectric materials for medical ultrasonic transducers. IEEE Ultrason Sym 1985;2:642–7.

[2] Shaulov AA, Smith WA, Ting RY. Modified-lead-titanate/polymer composites for hydrophone applications. Ferroelectrics 1989;93:177–82.
[3] Dunn ML. Micromechanics of coupled electroelastic composites: effective thermal expansion and pyroelectric coefficients. J Appl Phys 1993;73(10):5131–40.
[4] Ryu J, Priya S, Uchino K, Kim HE. Magnetoelectric effect in composites of magnetostrictive and piezoelectric materials. J Electroceram 2002;8: 107–19.
[5] Huang JH. Micromechanics determinations of thermoelectroelastic fields and effective thermoelectroelastic moduli of piezoelectric composites. Mater Sci Eng B 1996;39(3):163–72.
[6] Benveniste Y, Dvorak GJ. Uniform fields and universal relations in piezoelectric composites. J Mech Phys Solids 1992;40(6):1295–312.
[7] Biao W. Three-dimensional analysis of an ellipsoidal inclusion in a piezoelectric material. Int J Solids Struct 1992;29(3):293–308.
[8] Dunn ML, Taya M. Micromechanics predictions of the effective electroelastic moduli of piezoelectric composites. Int J Solids Struct 1993;30(2):161–75.
[9] Fakri N, Azrar L, El Bakkali L. Electroelastic behavior modeling of piezoelectric composite materials containing spatially oriented reinforcements. Int J Solids Struct 2003;40(2):361–84.
[10] Tan P, Tong L. Modeling for the electro-magneto-thermo-elastic properties of piezoelectric–magnetic fiber reinforced composites. Compos Part A—Appl Sci Manuf 2002;33(5):631–45.
[11] Aboudi J. Micromechanical prediction of the effective coefficients of thermo-piezoelectric multiphase composites. J Intel Mater Syst Struct 1998;9(9):713–22.
[12] Bravo-Castillero J, Guinovart-Díaz R, Sabina FJ, Rodríguez-Ramos R. Closed-form expressions for the effective coefficients of a fiber-reinforced composite with transversely isotropic constituents II. Piezoelectric and square symmetry. Mech Mater 2001;33(4):237–48.
[13] Tang T, Yu W. Variational asymptotic micromechanics modeling of heterogeneous piezoelectric materials. Mech Mater 2008;40(10):812–24.
[14] Tong ZH, Lo SH, Jiang CP, Cheung YK. An exact solution for the three-phase thermo-electro-magneto-elastic cylinder model and its application to piezoelectric–magnetic fiber composites. Int J Solids Struct 2008;45(20):5205–19.
[15] Levin VM, Rakovskaja MI, Kreher WS. The effective thermoelectroelastic properties of microinhomogeneous materials. Int J Solids Struct 1999;36(18):2683–705.
[16] Olson GB. Designing a new material world. Science 2000;288(5468):993–8.
[17] Lipinski P, Barhdadi EH, Cherkaoui M. Micromechanical modeling of an arbitrary ellipsoidal multi-coated inclusion. Philos Mag 2006;86(10):1305–26.
[18] Koutsawa Y, Cherkaoui M, Daya EM. Multi-coating inhomogeneities problem for effective viscoelastic properties of particulate composite materials. J Eng Mater Technol 2008;131(2):021012.
[19] Berger H, Kari S, Gabbert U, Rodríguez-Ramos R, Bravo-Castillero J, Guinovart-Díaz R. A comprehensive numerical homogenisation technique for calculating effective coefficients of uniaxial piezoelectric fibre composites. Mater Sci Eng: A 2005;412(1-2):53–60.
[20] Berger H, Kurukuri S, Kari S, Gabbert U, Rodríguez-Ramos R, Bravo-Castillero J, et al. Numerical and analytical approaches for calculating the effective thermo-mechanical properties of three-phase composites. J Therm Stress 2007;30(8):801–17.
[21] Chan HW, Unsworth J. Simple model for piezoelectric ceramic/polymer 1–3 composites used in ultrasonic transducer applications. IEEE Trans Ultrason Ferr Freq Cont 1989;36(4):434–41.
[22] Tessier-Doyen N, Grenier X, Huger M, Smith DS, Fournier D, Roger JP. Thermal conductivity of alumina inclusion/glass matrix composite materials: local and macroscopic scales. J Eur Ceram Soc 2007;27(7):2635–40.
[23] Barnett DM, Lothe J. Dislocations and line charges in anisotropic piezoelectric insulators. Phys Status Solidi B 1975;67:105–11.
[24] Zeller R, Dederichs PH. Elastic constants of polycrystals. Phys Status Solidi B 1973;55:831–42.
[25] Eshelby JD. Elastic inclusions and inhomogeneities. Progress in Solid Mechanics, vol. 2. Amsterdam: North-Holland; 1961.
[26] Walpole LJ. Elastic behavior of composite materials: theoretical foundations. Adv Appl Mech 1981;21:169–242.
[27] Cherkaoui M, Sabar H, Berveiller M. Micromechanical approach of the coated inclusion problem and applications to composite materials. J Eng Mater Technol 1994;116:274–8.
[28] Mikata Y. Determination of piezoelectric Eshelby tensor in transversely isotropic piezoelectric solids. Int J Eng Sci 2000;38(6):605–41.
[29] Wu TL, Huang JH. Closed-form solutions for the magnetoelectric coupling coefficients in fibrous composites with piezoelectric and piezomagnetic phases. Int J Solids Struct 2000;37(21):2981–3009.
[30] Broohm A, Zattarin P, Lipinski P. Prediction of mechanical behaviour of inhomogeneous and anisotropic materials using an incremental scheme. Arch Mech 2000;52(6):949–67.
[31] Li JY. Thermoelastic behavior of composites with functionally graded interphase: a multi-inclusion model. Int J Solids Struct 2000;37(39):5579–97.